CHAPTER-I

INTRODUCTION

1.0 ELECTRON SPIN RESONANCE

Electron spin resonance (ESR) or otherwise known as electron paramagnetic resonance (EPR) spectroscopy is the resonant absorption of microwave radiation by an unpaired electron of an atom or molecule, such as organic and inorganic free radicals or inorganic complexes possessing a transition metal ion when placed in a strong magnetic field. The method of electron spin resonance was discovered in 1944 in Kazan University by E. Zavoisky in the course of investigations of electromagnetic energy absorption by paramagnetic metal salts [1]. ESR spectroscopy has been applied to different disciplines and research areas including physics, chemistry, biology, medicine and geology since it is a most direct and sensitive method to study paramagnetic species [2-5]. ESR can be used to obtain structural information of molecules together with details about their electron density distributions. In solutions and solids, the dynamics of molecules and the kinetics of chemical reactions can be studied. Spectral features, such as resonance frequencies, splittings, line shapes and line widths are sensitive to the electronic distribution, molecular orientations, nature of the environment, and molecular motions [6].

1.1 PRINCIPLE OF ESR

Many researchers reviewed the basis of the ESR theory [7-14]. The degeneracy of the electron spin energy levels is lifted, when an electron is placed in a magnetic field. Fig. 1.1 shows the energy levels of an electron placed in a magnetic field, which is described by the spin Hamiltonian

$$\hat{H}_s = g\,\mu_B\,\mathbf{B}.\mathbf{S}_z \qquad (1.1)$$

\where g is called the g-factor ($g_e = 2.00232$ for a free electron), μ_B is the Bohr magneton (9.274×10^{-24} JG^{-1}), B is the magnetic field strength in gauss, and S_z is the z-component of the spin angular momentum operator (the field defines the z-direction). The electron spin energy levels are easily found by application of $\hat{H}_s$ to the electron spin eigen functions corresponding to $m_s = \pm 1/2$:

$$\hat{H}_s \left|\pm 1/2\right\rangle = \pm 1/2\, g\, \mu_B B \left|\pm 1/2\right\rangle = E_{\pm}\left|\pm 1/2\right\rangle \qquad (1.2)$$

Thus

$$E_{\pm} = \pm 1/2\, g\,\mu_B B \qquad (1.3)$$

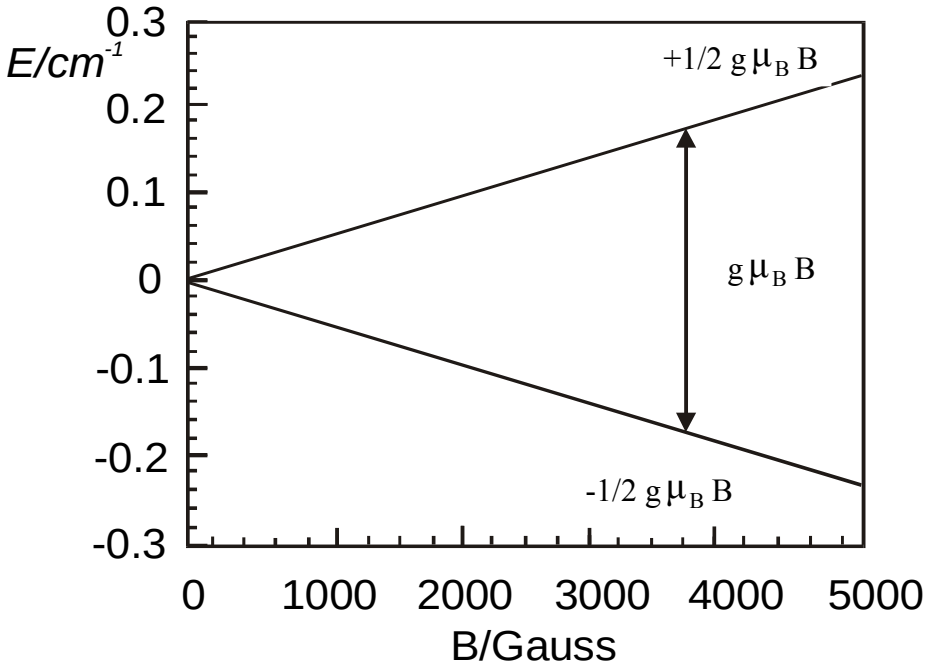

Fig. 1.1 Energy levels of an electron placed in a magnetic field.

The difference in energy between the two levels is given by

$$\Delta E = E_+ - E_- = g\,\mu_B B \qquad (1.4)$$

The arrow shows the transitions in Fig. 1.1 corresponds to the energy of a photon required to cause a transition

$$h\nu = g\mu_B B \tag{1.5}$$

or in wavenumbers

$$\bar{\nu} = \frac{g\mu_B B}{hc} \tag{1.6}$$

where h is the plank's constant and c is the velocity of light. The ESR absorption signal is detected corresponding to the resonance magnetic field, when the resonance condition is fulfilled.

1.2 BOLTZMANN DISTRIBUTION AND LARMOR PRECESSION

The macroscopic assembly containing a generic number of electrons is analyzed and not only a single spin during an ESR experiment. In thermal equilibrium, the distribution of spins over the possible states is statistical and governed by the Boltzmann's distribution law, by the following relation

$$N_+ = N_- \cdot e^{-\Delta E/k \cdot T} \tag{1.7}$$

where N_- and N_+ are the number of spins in the lower and upper energy states, ΔE is the energy difference given in equation, k is the Boltzmann's constant and T is the absolute temperature. For electrons in a field of 9.5 GHz (X band) and at room temperature (298 K), the populations of the two spin states can be calculated, which differs by only 1.5 parts in 10^3. At low temperature, the difference between the two states can be enhanced and thus the increase in ESR signal can be obtained.

In most systems, electrons occur in pairs such that the net magnetic moment is zero. Hence only species that contain one or more unpaired

electrons possess the net spin necessary for suitable interaction with an electromagnetic field. ESR transitions between the electron spin levels occur only, when there is a population difference between the spin states, the magnetic component of the electromagnetic radiation is perpendicular to the steady field B_0 and the following selection rule is fulfilled for spin transitions

$$\Delta m_s = \pm 1 \tag{1.8}$$

The behavior of a spinning electron can be considered analogous to that of a gyroscope revolving in friction free bearings. The magnetic moment vectors of spin dipoles starts precessing around the magnetic field in a cone in anticlockwise direction to the field at a uniform angular velocity ω_0 making a constant angle with the field. This motion is called the Larmor precession of the spin

$$\omega_0 = \gamma B_0 \tag{1.9}$$

where, ω_0 is known as the Larmor frequency and γ is the gyromagnetic ratio. The potential energy of the spinning particles remains constant in this precession. This potential energy can be changed by changing the orientation angle of the magnetic moment vector to the other permitted angle. This can be achieved by applying a secondary magnetic field rotating around the main field with a frequency equal to Larmor frequency. Under this condition, the rotating magnetic field is in resonance with the precessing magnetic field and thus induces a transition from one level to the other level. This is a mechanism by which particle spins can interact with a beam of electromagnetic radiation. If the beam has the same frequency as that of the precessing particle, it can interact coherently with the particle and energy can be exchanged. The ESR signals can be achieved by two ways; one is by varying the field strength keeping the frequency of the oscillator constant and another by varying the

frequency of the oscillator, keeping the external magnetic field constant. The second method is experimentally more favorable because it is relatively easy to vary the magnetic field (i.e., the current in the electromagnet) than to vary the frequency of radiation beam. Hence, an ESR spectrum is observed by placing the paramagnetic centre in a magnetic field and the electrons caused to resonate between the two states and the energy absorption is monitored. The magnetic field where this absorption occurs is known as resonance field, which is shown in Fig. 1.1.

1.3 SENSITIVITY

As for any quantum mechanical system interacting with electromagnetic radiation, a photon can induce either absorption or emission. The experiment detects net absorption, i.e., the difference between the number of photons absorbed and the number emitted. Since absorption is proportional to the number of spins in the lower level and emission is proportional to the number of spins in the upper level, the net absorption is proportional to the difference

Net absorption α $N_- - N_+$

The ratio of populations at equilibrium is given by the Boltzmann distribution

$$\frac{N_+}{N_-} = e^{-\Delta E/k_B T} = e^{-g\mu_B B/k_B T} \tag{1.10}$$

For ordinary temperatures and ordinary magnetic fields, the exponent is very small and the exponential can be accurately approximated by the expansion, $e^{-x} \approx 1 - x$. Thus the above equation can be written as

$$\frac{N_+}{N_-} \approx 1 - \frac{g\mu_B B}{k_B T} \tag{1.11}$$

Since $N_- \approx N_+ \approx N/2$, the population difference can be written as

$$N_- - N_+ = N_-\left[1-\left(1-\frac{g\mu_B B}{k_B T}\right)\right] = \frac{Ng\mu_B B}{2k_B T} \tag{1.12}$$

The above equation shows that the ESR sensitivity (net absorption) increases with decreasing temperature and increasing magnetic field strength. The magnetic field is proportional to microwave frequency, in principle sensitivity should be greater for K-band or Q–band spectrometers than X-band.

1.4 TOTAL HAMILTONIAN

1.4.1 Electron Zeeman energy

This represents the direct interaction between the electron spin magnetic moment μ_s and the external magnetic field B, which is given by

$$H_{SB} = -\mu_s \cdot \mathbf{B} = g\mu_B \mathbf{S}\cdot\mathbf{B} \tag{1.13}$$

1.4.2 Nuclear Zeeman energy

This is the interaction energy of the magnetic moment μ_I of the nucleus and the external magnetic field, which is given by

$$H_{IB} = -\mu_I \cdot B = -g_N\mu_N \mathbf{I}\cdot\mathbf{B} \tag{1.14}$$

where g_N is the nuclear g-factor and μ_N is the nuclear magneton.

1.4.3 Nuclear-electron spin coupling

Interaction of the unpaired electron with the magnetic moments of the nuclei gives rise to two additional terms, the nuclear electron spin coupling and Fermi contact term. The splitting of the spectrum observed due to this is called the hyperfine structure. The nuclear electron coupling is a direct dipole-dipole interaction between the electron and nuclear magnetic moments. As this

interaction depends upon the angle between the magnetic field and the line joining the two dipoles, it is directional and is referred to as the anisotropic interaction. Its magnitude is proportional to $1/r^3$ where r is the distance between the dipoles. For free radicals in solution, since the orientation of the radicals with respect to the magnetic field changes rapidly, this interaction averages to zero and the hyperfine structure observed. The dipole-dipole interaction is given by

$$H_{dip} = gg_N\mu_B\mu_N\left[\frac{S \bullet I}{r^3} - \frac{3(S \bullet r)(I \bullet r)}{r^5}\right] \tag{1.15}$$

The second electron-nuclear interaction is the Fermi contact interaction which has no classical analogue. This represents the interaction between the nuclear moment and the magnetic field produced by the electron spin at the nucleus. This depends on the finite unpaired electron density at the nucleus which is possible when it occupies an s-orbital.

$$H_F = \frac{8\pi}{3} gg_N\mu_B\mu_N|\psi(0)|^2 S \bullet I = aS \bullet I \tag{1.16}$$

where $\psi(0)$ is the electron wave function at the center of the nucleus and 'a' is the hyperfine splitting constant

$$a = \frac{8\pi}{3} gg_N\mu_B\mu_N|\psi(0)|^2 \tag{1.17}$$

since the Fermi contact term involves only s electrons, the hyperfine splitting constant is isotropic.

1.5 HYPERFINE STRUCTURE

When one or more magnetic nuclei interact with the unpaired electron, the perturbation of the electron energy term is included in the spin Hamiltonian

$$\hat{H}_s = g\mu_B \mathbf{B}\cdot\mathbf{S_z} + a\mathbf{I}\cdot\mathbf{S} \tag{1.18}$$

The above equation can be expanded by using the dot product and substituting the raising and lowering operators for S_x, S_y, I_x, and I_y ($\hat{S}_\pm = \hat{S}_x \pm i\hat{S}_y, \hat{I}_\pm = \hat{I}_x \pm i\hat{I}_y$). Thus, the equation (1.18) can be written as

$$\hat{H}_s = g\mu_B \mathbf{B}\cdot\mathbf{S}_z + a\mathbf{I}_z\cdot\mathbf{S}_z + \frac{1}{2}(\hat{I}_+\hat{S}_- + \hat{I}_-\hat{S}_+) \tag{1.19}$$

Suppose that the nuclear spin is 1/2 ; operating on the spin functions, $|m_s, m_1\rangle$,

$$\hat{H}_s\left|\frac{1}{2},\frac{1}{2}\right\rangle = \left(\frac{1}{2}g\mu_B B + \frac{1}{4}a\right)\left|\frac{1}{2},\frac{1}{2}\right\rangle \tag{1.20}$$

$$\hat{H}_s\left|\frac{1}{2},\frac{-1}{2}\right\rangle = \left(\frac{1}{2}g\mu_B B - \frac{1}{4}a\right)\left|\frac{1}{2},-\frac{1}{2}\right\rangle + \frac{1}{2}a\left|-\frac{1}{2},\frac{1}{2}\right\rangle \tag{1.21}$$

$$\hat{H}_s\left|\frac{-1}{2},\frac{1}{2}\right\rangle = \left(-\frac{1}{2}g\mu_B B - \frac{1}{4}a\right)\left|-\frac{1}{2},\frac{1}{2}\right\rangle + \frac{1}{2}a\left|\frac{1}{2},-\frac{1}{2}\right\rangle \tag{1.22}$$

$$\hat{H}_s\left|\frac{-1}{2},\frac{-1}{2}\right\rangle = \left(-\frac{1}{2}g\mu_B B + \frac{1}{4}a\right)\left|\frac{-1}{2},\frac{-1}{2}\right\rangle \tag{1.23}$$

The Hamiltonian matrix is

$$\begin{pmatrix} \frac{1}{2}g\mu_B B + \frac{1}{4}a & 0 & 0 & 0 \\ 0 & \frac{1}{2}g\mu_B B - \frac{1}{4}a & \frac{1}{2}a & 0 \\ 0 & \frac{1}{2}a & -\frac{1}{2}g\mu_B B - \frac{1}{4}a & 0 \\ 0 & 0 & 0 & -\frac{1}{2}g\mu_B B + \frac{1}{4}a \end{pmatrix} \tag{1.24}$$

If the hyperfine coupling is sufficiently small, $a << g\mu_B B$, the diagonal elements, which correspond to the energies in first–order perturbation theory

$$E = \pm\frac{1}{2}g\mu_B B \pm \frac{1}{4}a \tag{1.25}$$

However, for large a, the matrix must be diagonalized. This is easy when there is only one hyperfine coupling

$$E\left(\frac{1}{2},\frac{1}{2}\right) = \frac{1}{2}g\mu_B B + \frac{1}{4}a \tag{1.26}$$

$$E\left(-\frac{1}{2},-\frac{1}{2}\right) = -\frac{1}{2}g\mu_B B + \frac{1}{4}a \tag{1.27}$$

$$E\left(\frac{1}{2},\frac{-1}{2}\right) = \frac{1}{2}g\mu_B B\sqrt{1+\left(\frac{a}{g\mu_B B}\right)^2} - \frac{1}{4}a \tag{1.28}$$

$$E\left(\frac{-1}{2},\frac{1}{2}\right) = -\frac{1}{2}g\mu_B B\sqrt{1+\left(\frac{a}{g\mu_B B}\right)^2} - \frac{1}{4}a \tag{1.29}$$

These equations are a special case of the general solution to equation called the Breit–Rabi equation.

For nitroxide radicals, since ^{14}N has a spin angular moment I = 1 and resulting spin quantum number m_I = 1, 0 and -1, the degenerate spin state is splits into two Zeeman sub-levels and further split into six energy states. Based on the ESR selection rules $\Delta m_s=\pm1$ and $\Delta m_I=0$, there are three allowed transitions leading to a triplet ESR spectrum, which is shown in Fig. 1.2a. Similarly, Fig. 1.2b shows the energy level diagram of hyperfine interaction on a system with one unpaired electron (S=1/2) and one nucleus with I=1/2. Typically, the interactions of an unpaired electron with n equivalent nuclei having nuclear spin I lead to 2nI+1 lines in the ESR spectrum [11].

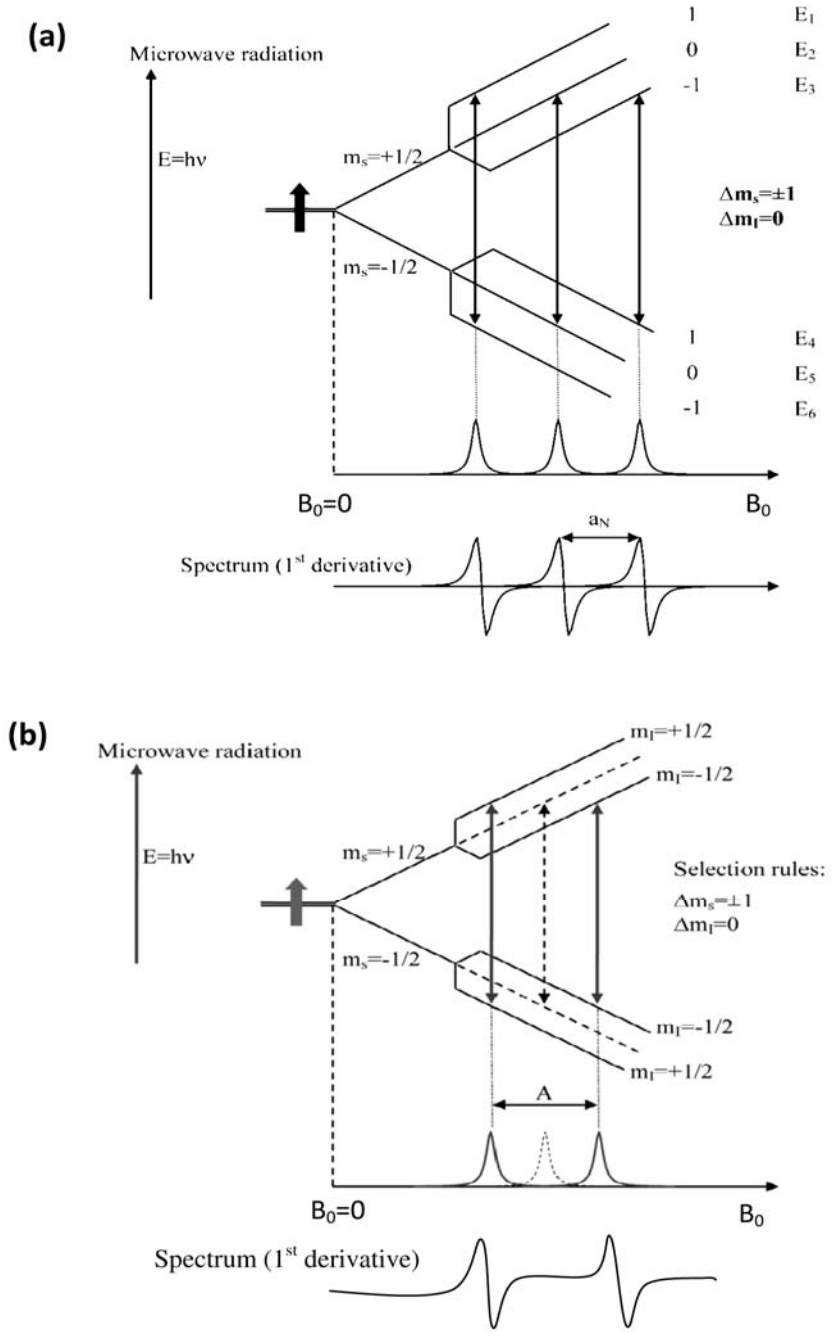

Fig. 1.2 (a) The energy level diagram and ESR spectrum for a nitroxyl radical (S = 1/2 and I= 1) (b) Energy level diagram of hyperfine interaction on a system with on unpaired electron (S=1/2) and on nucleus with I=1/2.

1.6 ISOTROPIC SPECTRUM

An isotropic ESR spectrum, which is the spectrum of a freely tumbling radical in liquid solution can contain several kinds of useful information's:

i) The hyperfine coupling pattern provides information on the numbers and kinds of magnetic nuclei with which the unpaired electron interacts.

ii) The spacing of the lines and the center of gravity of the spectrum yield the hyperfine coupling constants A and g-value, which is related to the way in which the unpaired electron spins density, is distributed in the molecule.

iii) The integrated intensity of the spectrum is proportional to the concentration of radicals in the sample.

iv) The spectral line widths are related to the rate of the rotational motions, which average anisotropies in the g- and hyperfine matrices.

v) The saturation behavior of a spectrum, which is also related to the spin-lattice relaxation time, a measure of the rate of energy transfer between the electron spin and its surroundings.

1.7 LINE POSITIONS IN ISOTROPIC SPECTRA

ESR spectra of radicals in liquid solution are usually interpreted in terms of a spin Hamiltonian, which is given in equation (1.18). The spectral information is contained in the parameters, g-factor, and A_i, the electron–nuclear hyperfine coupling constant for nucleus i. Using spin functions based on quantum numbers m_s and m_i, equation (1.18) can be used to compute the energy levels. Equating energy differences for the allowed transitions $(\Delta m_s = \pm 1, \Delta m_i = 0)$ with the microwave photon energy,

$$E_{(m_s = 1/2)} - E_{(m_s = -1/2)} = h\upsilon \qquad (1.30)$$

According to first-order perturbation theory, the resonant magnetic field can be deduced and given as follows:

$$B = B_o - \sum_i a_i m_i \quad (1.31)$$

where, $B_0 = h\nu/g\mu_B$ represents the center of the spectrum and $a_i = A_i/g\mu_B$ is the hyperfine coupling constant in field units.

1.8 ANISOTROPIC ESR SPECTRA

The anisotropies lead to the line broadening in isotropic ESR spectra, which influence solid state spectra more directly. Accordingly, a more complex spin Hamiltonian is required to interpret such spectra, which is given in equation (1.18). In general, the g and A_i are diagonal along the principal axes of a coordinate system.

When a radical is oriented such that the magnetic field direction is located by the polar and azimuthal angles, θ and ϕ, relative to the g-matrix principal axes, the resonant field is given according to first order perturbation theory

$$B = B_o - a_i m_i/g\mu_B \quad (1.32)$$

$$B_0 = h\nu/g\mu_B \quad (1.33)$$

where,

$$g^2 = g_x^2 \sin^2\theta \cos^2\Phi + g_y^2 \sin^2\theta \sin^2\Phi + g_z^2 \cos^2\theta$$

$$a_i^2 = a_{iz}^2 S_{ix}^2 + a_{iy}^2 S_{iy}^2 + a_{iz}^2 S_{iz}^2$$

$$S_{ik} = [g_x \sin\theta \cos\Phi\, l_{ixk} + g_y \sin\theta \cos\Phi\, l_{iyk} + g_z \cos\theta\, l_{izk}]/g$$

where l_{ijk} are direction cosines indicating the orientation of the k^{th} principal axis of the i^{th} hyperfine matrix relative to the j^{th} g-matrix principal axis.

1.9 RELAXATION

The mechanism by which excess spin energy of a system is shared either with the surroundings or with other nuclei or electron is referred to as relaxation process; the time taken for a fraction 1/e = 0.37 of the excess energy to be dissipated is called relaxation time. Two different relaxation processes can occur both for nuclei and electrons.

1.9.1 Spin-Lattice Relaxation

In this case, the excess spin energy equilibrates with the surroundings (the lattice) by spin-lattice relaxation time (or longitudinal relaxation time) denoted as T_1. This is a non-radiative transfer of energy from spins to the other degree of freedom (lattice). This type of relaxation comes about by lattice motions. For example, atomic vibrations in a solid lattice, or molecular tumbling in liquids and gases. The relaxation time is described by a single exponential decay. The relaxation time along the direction of a static magnetic field B_0 is called the longitudinal relaxation time T_1. The longitudinal relaxation is accompanied by a change of the energy of the spin system. The thermal motion is the source and sink of energy exchange in the relaxation processes. In solids, thermal motion is usually described by phonons, which are quanta (photons) with energies in the range corresponding to lattice vibrations. The longitudinal relaxation is caused by absorption or stimulated emission of phonons. Therefore, the coupling between the spin system and lattice is required for the longitudinal relaxation, which is often called spin-lattice relaxation. The term lattice comes from its use in early studies performed with ionic lattices. However, the usage has been generalized and refers to degrees of freedom other than those directly concerned with spin. The phonons have a spectrum of frequencies that range over many orders of magnitudes with varying intensities. However, only those fluctuations with frequencies that

match the ESR frequency are capable of inducing transitions. There are several mechanisms by which the spin-lattice interaction can take place in condensed phases; these are called direct, Raman and Orbach processes. These processes involve interaction of the spin system with phonons of the lattice. The spin-lattice relaxation is efficient at room temperature (10^{-6} s) but becomes progressively less at reduced temperature, often becomes several minutes at the temperature of liquid nitrogen.

1.9.2 Spin-Spin Relaxation

There is sharing of excess spin energy directly between spins of nuclei or electrons, via spin-spin relaxation (or transverse relaxation), spin-spin relaxation time is denoted as T_2. The relaxation time in the plane perpendicular to the static magnetic field B_0 is the transverse relaxation time T_2. In the absence of a microwave field, the equilibrium magnetization components M_x and M_y are zero, but these components appear in the presence of the microwaves with a magnetic field of amplitude B_1 orthogonal to the field B_0. The transverse relaxation occurs without the exchange of energy with the lattice. The transverse relaxation is concerned with the mutual spin flips caused by interactions within the ensemble of spins in the sample and thus is often called spin-spin relaxation. The main consequence of these relaxation processes (T_1 and T_2) determines the line shape of the spectrum (the unique resonance line) of the two-level system. This kind of relaxation is very effective even at low temperature, unless the system is extremely dilute and gives a relaxation of 10^{-8} - 10^{-6} s.

1.10 LINE SHAPES

The shapes of ESR lines are usually described by Lorentzian and Gaussian line shapes and their derivatives. ESR lines are usually observed as Lorentzian in line shapes for liquids, if there is no hyperfine broadening, the

concentration of paramagnetic centers is low and there is dynamic averaging. Lorentzian line can be described by the distribution given below and is shown in the Fig. 1.3.

$$g(\omega) = \frac{T_2}{\pi} \cdot \frac{1}{1 + T_2^2 \cdot (\omega - \omega_0)} \tag{1.34}$$

where g(ω) is function of frequency, ω_0 is resonance frequency and T_2 is transverse relaxation time. The Gaussian shapes for lines are observed if the line is a superposition of many components. Generally, the unpaired electrons in a sample are not all subjected to exactly same magnetic field. Thus at any time, only a small fraction of the spins is in resonance as the external magnetic field is swept. The observed line is then a superposition of a large number of individual components each slightly shifted from the others thus giving rise to Gaussian curve. This phenomenon is also called inhomogeneous broadening, which is due to the inhomogeneous external magnetic field, unresolved hyperfine structure, anisotropic interactions in randomly oriented systems in the solid state giving rise to highly unsymmetrical line shapes and dipolar interactions with other fixed paramagnetic centers. The expression is given as follows

$$g(\omega) = \frac{T_2}{\sqrt{2\pi}} e^{-\frac{1}{2}T_2^2(\omega-\omega_0)^2} \tag{1.35}$$

The Gaussian curve along with its derivative is shown in Fig.1.3.

The main parameters describing these lines are; the maximum amplitude (Y_{max}) or the maximum height of the observed line, this factor depends on the experimental factors such as power level, detector sensitivity, amplifier settings, sample composition, temperature and the half width at half height (Γ). In ESR spectroscopy, the line shapes can therefore be described as Lorentzian, Gaussian or a mixture of both and spectral line widths are popularly given by peak to peak distance of first derivative spectrum, which is denoted as ΔB_{PP}.

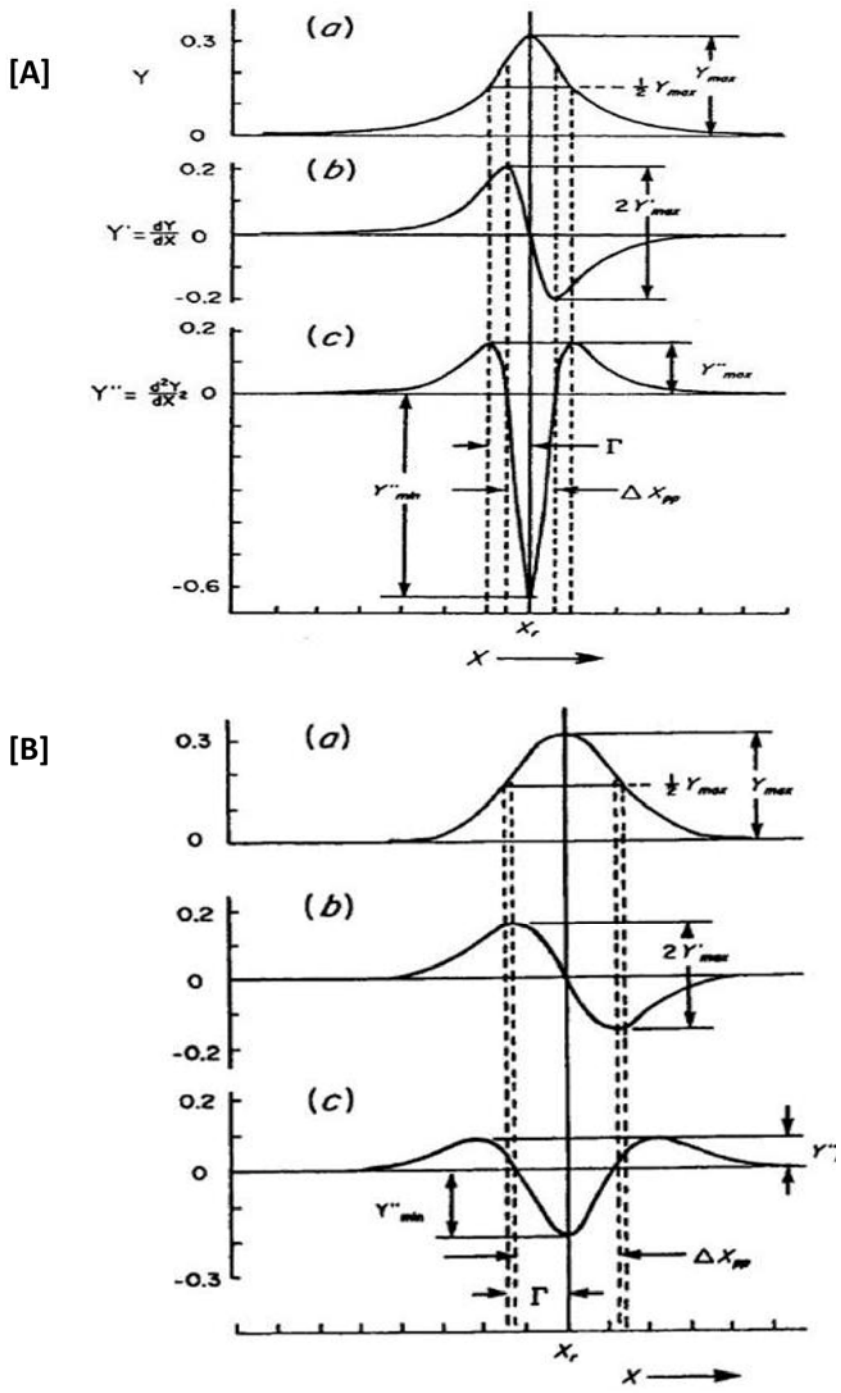

Fig. 1.3 Line shapes from Lorentzian function [A] and Gaussian function [B] and the respective (a) absorption, (b) first derivative and (c) second order derivative spectrum.

1.11 ROTATIONAL CORRELATION TIME

The electron spin resonance (ESR) spectroscopy is a powerful technique to obtain information about the rotational mobility of spin-labeled molecules, because a very broad range of molecules can be covered by this technique. The rotational correlation time τ_R is a parameter to express the mobility of spin probes in their environment. The τ_R can be obtained from the ESR spectral line width and relative intensities. The conventional ESR spectroscopy can detect changes in τ_R of spin probes ranging from 10^{-12} to10^{-9} s, which corresponds to the lifetime of the probe in the given orientation. For rapid-tumbling radicals, the dipolar interactions average out to zero and hence the resulting ESR spectra are isotropic with g_{iso} and A_{iso} parameters. For instance, nitroxyl radicals in a dilute solution yield a triplet ESR spectrum with the three lines of similar height Fig.1.4a. In the cases, where the tumbling of the nitroxyl radical is restricted (*e.g.* bonded to a metal surface), the high field line is broadened Fig. 1.4b.

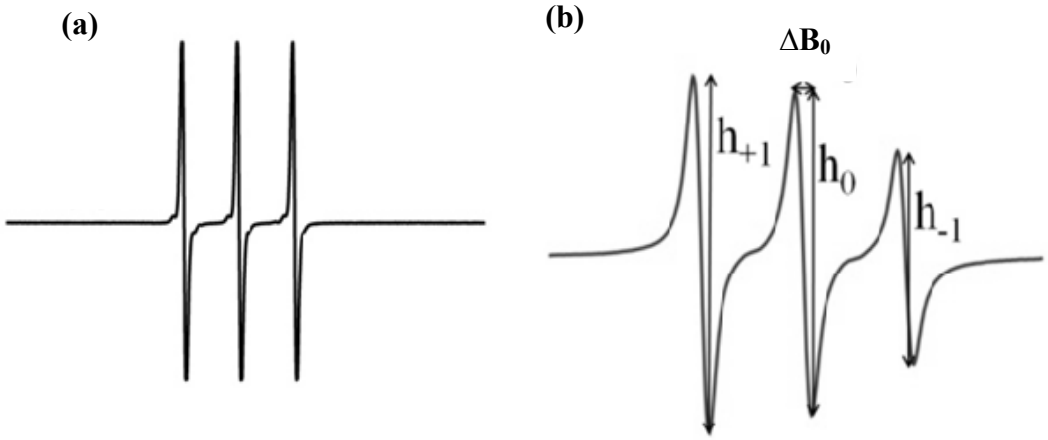

Fig. 1.4 ESR spectra of a free nitroxyl radical in (a) dilute solution and (b) nitroxyl radical bonded to metal surfaces

The rotational correlation time τ_R(s) can be obtained by the method of Knowles et al. [15-18]

$$\tau_R = 6.5 \times 10^{-10} \Delta B_0 [(h_0/h_{-1})^{1/2}-1] \quad (1.36)$$

where h_{-1} and h_0 are the amplitudes of the high-field and central lines in the ESR spectra, respectively, and ΔB_0 is the line width of the central line in gauss. The rotational motion of the spin probe was assumed to be isotropic.

The mobility of a spin probe depends on the local viscosity and tumbling of the macromolecule as a whole. The mobility can be quantified by the rotational correlation time τ_R, which corresponds to the typical time during which a molecule maintains its spatial orientation. If the inverse of τ_R is of the same order of magnitude as the anisotropy of an interaction, this anisotropy is partially averaged and the ESR spectrum depends strongly on τ_r and on specific dynamics, such as the preference for a particular rotational axis or restrictions on the motion. The nitroxyl radicals with $\tau_R < 4$ ns, give a liquid-type spectrum and are considered mobile (or fast), while nitroxyl radicals with $\tau_R > 4$ ns give a solid-type spectrum and are considered immobile (or slow).

1.12 OVERHAUSER-ENHANCED MAGNETIC RESONANCE IMAGING

1.12.1 Overhauser effect

Overhauser-enhanced Magnetic Resonance Imaging (OMRI) is based on the Overhauser effect (also known as dynamic nuclear polarisation, DNP), which was predicted by Overhauser (1953) and first demonstrated by Carver and Slichter (1956). This imaging method is a double resonance technique that uses the presence of paramagnetic agents to enhance the signal intensity from nuclear spins by means of a process known as dynamic nuclear polarisation (DNP) or Overhauser effect [19-23]. In this phenomenon, the relatively stronger magnetic moment of the electron is used to enhance the polarisation of nuclear spins, thereby enhancing their signal. The unique advantage of this technique is high spatial resolution of the image and short acquisition time. The significant contrast-to-noise ratio obtained by this technique makes OMRI advantageous in obtaining physiological information. OMRI is a promising

technique for imaging the distribution and dynamics of free radicals [24-26]. In DNP, the Nuclear magnetic resonance (NMR) signal of a solution is observed (often the proton NMR signal in water) while the ESR resonance of the paramagnetic solute irradiated. The ESR irradiation causes an enhancement in the NMR signal arising from parts of sample containing free radicals, and these regions exhibit altered intensity in the final image, revealing the distribution of the free radical. The maximum theoretically achievable DNP enhancement is given by half the ratio of the gyromagnetic ratios of the spins involved–which in this case are electrons and protons, giving a maximum value of -329 [27-29].

1.12.2 Phenomenological Description

The DNP in free radical solutions [30], which deals with interaction between the nuclear spins I in the solvent and electron spins S which are the solute's unpaired electrons. The rapid, random molecular motion in the solution will ensure that any nucleus will encounter many unpaired electrons on the time scale of nuclear relaxation, so that each nucleus can be considered to be in a constant interaction with an unpaired electron. Considering only pairs of electron and nuclear spins, and restricting the discussion of proton NMR (so that I=1/2 and S=1/2), it can be seen that there are four possible energy levels, denoted by $|m_s, m_I\rangle$ where m_I and m_S are the usual spin quantum numbers, the four states being $|+,-\rangle$, $|+,+\rangle$, $|-,-\rangle$, $|-,+\rangle$. This is illustrated in the energy-level diagram in Fig. 1.5, where the four states are also labeled as ❶, ❷, ❸, and ❹ in the order of decreasing energy. It should be noted that the actual energy difference between states ❶ and ❸ or ❷ and ❹ (ESR transitions) is approximately 660 times that between states ❶and ❷ or ❸and❹ (NMR transitions). The energy levels are also labeled with the population n_i of the state, which is indicated qualitatively by the thickness of the energy-level lines, a thicker lines indicating a higher population of the state.

The situation at thermal equilibrium is shown in Fig. 1.5a. The population of each state depends on its energy and is given by the familiar Boltzmann distribution. The level ❶ has the lowest population level ❹ the highest, and because of the much larger energies of electronic transitions relative to nuclear, the difference in population between states ❶ and ❷ is much smaller than that between ❶ and ❸.

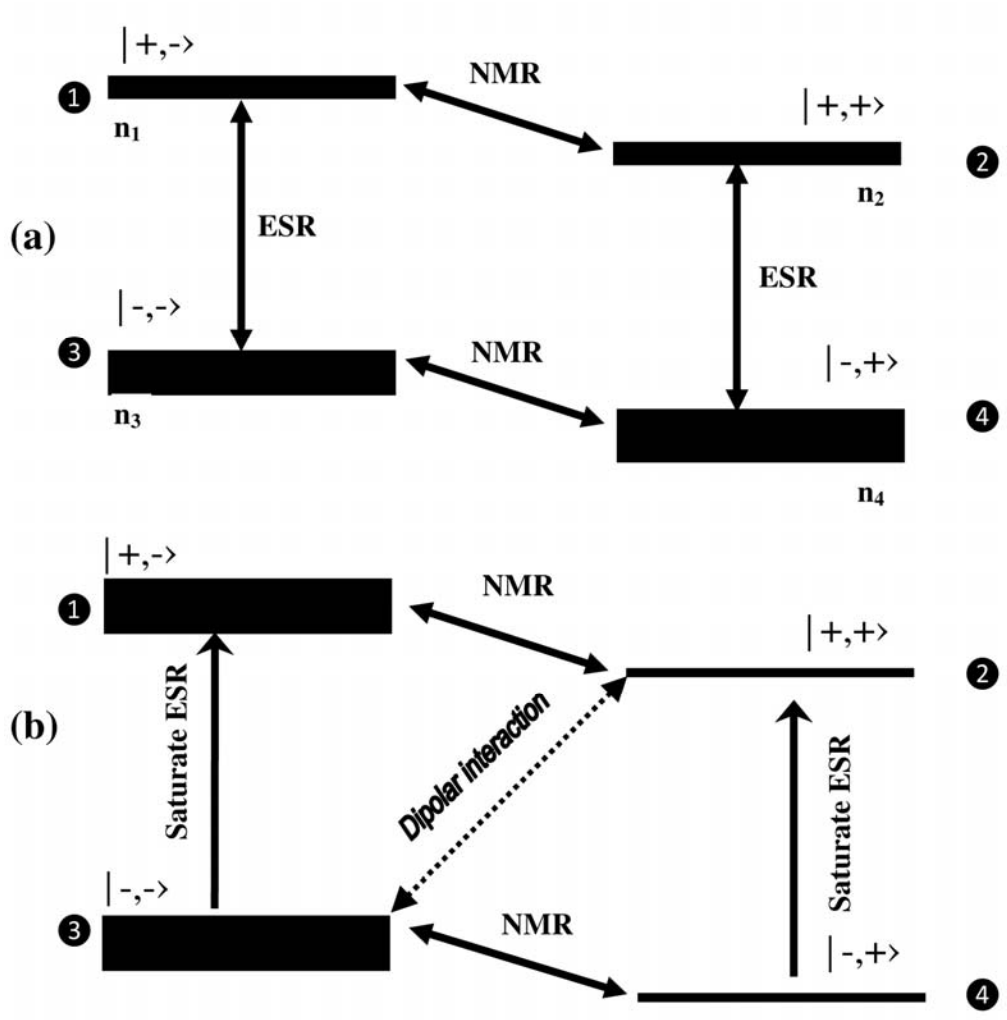

Fig. 1.5 Energy level diagrams for the two-spin nucleus-electron system, providing phenomenological description of the Overhauser effect (a) at thermal equilibrium; (b) while saturating the ESR transition.

Fig.1.5b shows the situation when the electron transitions (❸↔❶ and ❹↔❷) are irradiated. If the intensity of the ESR irradiation is sufficient, the ESR transitions will be saturated, causing an equalizing of the populations, $n_1 = n_3$ and $n_2 = n_4$. In a solution of rapidly-tumbling free radical molecules, the predominant interaction between unpaired electron and nuclear spins is a dipole- dipole interaction, the main result of which is simultaneous nuclear and electron spin flips, represented by transitions between the states ❷ and ❸ as shown. This cross-relaxation pathway will cause the relative populations of these states to confirm the Boltzmann distribution, and because there is a large energy difference between the states, the polarization will be large, i.e.$n_3 >> n_2$.

To examine the populations of the states between the nuclear transitions occur (❶↔❷ and ❸↔ ❹) it can be seen that the polarization is much greater than would normally be the case between these energy-levels. In fact, the polarization of the nuclear states is of the order of the electron states exhibit at thermal equilibrium. The transfer of polarization from electron to nuclear spins causes the DNP enhancement of the NMR signal amplitude. Furthermore, it can be seen that the nuclear polarization is actually opposite to that which is normally expected, with the upper energy states (❶ and ❸) having higher occupancy than the lower energy states (❷ and ❹). This population inversion is responsible for the phase change of the NMR signal upon ESR irradiation.

This simple discussion has neglect the fact that nuclear electron dipole-dipole interactions also cause other transitions to occur, namely ❶↔❷, ❸↔❹ and ❶↔❹. Nevertheless, transitions between levels ❷ and ❸ are dominant, and it can be shown that, taking into account the contributions of the other transitions mentioned, the largest possible enhancement factor of the NMR signal under these conditions is minus half the ratio of the gyromagnetic ratios, or -329.

1.12.3 DNP Theory

The enhancement factor E in a DNP experiment [19,20,31-33] can be defined as the ratio I_z/I_0 where I_z and I_0 are the NMR signals with and without ESR irradiation. The enhancement factor can be written as

$$E = 1 - \rho f s \frac{|\gamma_s|}{\gamma_I} \tag{1.37}$$

where γ_s and γ_I are respectively, the electronic and nuclear gyromagnetic ratios. The other variables in equation are ρ, the coupling factor *f,* the leakage factor and s, the saturation parameter of the ESR irradiation.

The coupling factor, ρ depends on the nature and time dependence of the nuclear-electron interactions. ρ takes the value -1 if the interactions are purely scalar, while ρ=1/2 if the interactions are entirely dipolar. In bio-medical applications of DNP deals with low concentrations of small rapidly tumbling free radical molecules in solution, the dipolar interactions are dominant, however the value ρ has been found to be dependent on the actual type of free radicals being studied.

The leakage factor, *f is* a measure of the fraction of nuclear relaxation arising from interactions with the free radicals unpaired electrons in solution. It can be written as

$$f = 1 - \frac{T_1}{T_1^0} \tag{1.38}$$

where T_1 is the NMR spin-lattice relaxation time of the free radical solution, T_1^0 is the spin-lattice relaxation time of the solution in the absence of free radical.

The saturation parameter, s, is a measure of degree of saturation of the ESR resonance, and depends on the strength of the ESR irradiation RF

magnetic field, B_2 and in the unpaired electron's ESR relaxation times, τ_1 and τ_2. The saturation factor can be written as

$$s = \frac{1}{n}\left(\frac{\gamma_s^2 B_2^2 \tau_1 \tau_2}{1+\gamma_s^2 B_2^2 \tau_1 \tau_2}\right) \tag{1. 39}$$

Where n is the number of lines in the free radical's ESR spectrum

If we assume that $\rho = 1/2$, then for proton NMR (with $\gamma_s/\gamma_I = 658$), we can rearrange equations (1.37)-(1.39) into the following expression.

$$E = 1 - \frac{329}{n\left(1+\frac{1}{\alpha P}\right)\left(1+\frac{1}{kcT_1^0}\right)} \tag{1.40}$$

The first two terms in the denominator are the reciprocal of the saturation parameter, and can be written in this way by assuming that $B_2^2 \alpha P$, where P is the power of the ESR irradiation, α being a constant of proportionality depending on the sample's ESR relaxation times and on the characteristics of the ESR resonator.

The second term in parenthesis on the denominator is the reciprocal of the leakage factor, which has been rewritten to specifically include the concentration, c, of the free radical solute and its longitudinal NMR relaxivity, k. This last term determines the DNP response as a function of free radical concentration, which is of considerable interest for biomedical applications of the technique.

Assuming that n = 3 (which is the case with nitroxide free radicals, for example), from equation (1.37) that the maximum enhancement factor, which would be obtained with complete saturation of ESR resonance (infinite ESR irradiation power) and high free radical concentration is $E^{max} = -109$. Although enhancement factors approaching this can be seen in aqueous solution of free

radicals, enhancement factors in DNP experiments with biological samples are normally at least a order of magnitude less than the above value.

1.13 SCOPE OF THE THESIS

Electron spin resonance spectroscopy is a powerful tool to study free radicals and paramagnetic metals ions in chemical and biological systems [34-36]. It is the direct and definitive technique for measuring and characterizing molecules with unpaired electron spin. ESR spectroscopy can be applied to obtain spatial information by utilizing magnetic field gradients in a manner similar to that of NMR Imaging. The most common spin labels are nitroxyl radicals due to their high persistency, distinctive hyperfine and g values. ESR offers the unique opportunity to perform non-invasive studies in nontransparent samples both in vivo and in vitro and has entered the fields of medicine and pharmacy during the last decade [37-40]. In detail, ESR was used to probe the microviscosity and micropolarity of systems, to characterize colloidal drug carriers, to monitor the microacidity in biodegradable polymers, and to follow drug release mechanisms [41,42].

Nitroxyl radicals have been widely used as antioxidants, contrast agents and spin probes [11, 43-45]. Spin labels are usually molecules containing the nitroxide moiety which possessed an unpaired electron localized on the nitrogen and oxygen atoms. These probes, or spin labels, are nitroxide derivatives containing an unpaired electron in the pp orbital of the N-O bond, the nitroxyl radical is stable owing to the presence of methyl groups on neighboring carbon atoms. The NO group is enclosed in either a six-membered piperidine or a five-membered pyrrole ring in order to limit flexibility. Pyrrole rings with an unsaturated bond are the least flexible. The unpaired electron in the pp orbital also interacts with the spin of the nitrogen nucleus, splitting the ESR signal into resonances corresponding to different nitrogen nuclear manifolds. Thus, the number of resonant peaks depends on the nitrogen isotope, three for ^{14}N and two for ^{15}N. The ^{15}N labels have the advantage of less

spectral dispersion which increases the signal amplitude 1.5-fold in conventional ESR. Nitroxyl radicals have also been widely used as spin probes for low frequency in vivo/in vitro electron spin resonance imaging (ESRI), and as contrast agents for Overhauser-enhanced magnetic resonance imaging (OMRI) [46-51].

In vivo ESR spectroscopy work began in the early 1980s, working mostly at L-band microwave frequencies with modified home-made cavity systems. The first major experiment was successfully achieved at the NIH ESR Center at the Medical College of Wisconsin, where the loop-gap resonator was adapted for ESR by Froncisz and Hyde [52]. Lukiewicz et al. [53] demonstrated direct in vivo observation of melanin free radicals in a melanoma tumor implanted in the tail of a live mouse. Berliner and Fujii published in vivo ESR studies using a single turn flat loop coil working at L-band (around 1.5 GHz), succeeding in detecting nitroxide ESR signals from plants and small animals doped with nitroxide spin probes [54-56]. Ono et al. modified and improved the original loop-gap resonator by avoiding the dielectric losses from the inserted small animal [57]. In addition, several resonator prototypes have been constructed in the 1-4 GHz frequency range by Sotgiu's group [58]. Swartz and Walczak developed a modified ring resonator as this device is useful in measuring tissues oxygen consumption [59]. Hirata et al. developed an improved external loop resonator with an automatic matching control system for in vivo ESR [60]. This loop resonator system allows one to measure an ESR signal while compensating perturbations due to movement of the subject animal. This modified system appears to be potentially valuable in applying in vivo ESR to human subjects, where the need to reduce noise from movements is also a major concern. ESR imaging however is faced with a number of technical problems, which make this technique more difficult to achieve in practice than that of NMR. The line widths of ESR signals are 3

orders of magnitude larger than those of NMR signals, and hence ESR imaging requires 100-1000 times more powerful gradients.

The signal decay of the spin probes depends on the oxidative stress in the living body. ESR CT imaging of spin probes should provide information on the distribution of oxidative stress in the living body [61]. H. Yokoyama et al. used the Blood brain barrier (BBB) permeable MC-PROXYL and impermeable carbamoyl-PROXYL to assess the three dimensional ESR images of the head of rats and mice [62]. Recently, the researchers observed the evidence of OH generation in the lungs of living mice after intracheal instillation of diesel exhaust particles, using non invasive L-band ESR spectroscopy and a membrane-impermeable nitroxyl probe [63]. H. Utsumi et al. observed the generation sites of reactive oxygen species (ROS) in rats idomethacin induced gastric ulcer using in vivo 300 MHz spectroscopy and nitroxyl probes with membrane permeability [64].

Electron spin resonance imaging (ESRI) technique provides functional information, the in vivo behavior of redox probes was found to accurately reflect redox status in several oxidative disease models. Proton-electron double resonance imaging (PEDRI) is one of the promising noninvasive methods to indirectly measure the concentration of oxygen. In this technique, proton MRI is acquired while irradiating and saturating the electron spin system. This double resonance technique couples the spatial resolution of MRI with the functional sensitivity of ESR. As a result, NMR signal intensity of the magnetically coupled water protons can be significantly increased in the regions where the paramagnetic probe is present. Enhancement of the nuclear polarization in solutions occur via dipole-dipole interaction and depends on several factors, such as (1) ESR spectral characteristic; (2) concentration of paramagnetic probe; (3) relaxivity in the solution; (4) electron relaxation times of the probe; and (5) applied RF power for ESR saturation.

Lurie et al. used nitroxyl radicals and successfully obtained images of tissue water protons in the vicinity of the paramagnetic radicals and so achieved in vivo imaging revealed that the dependence of image intensity on the proton mobility within biological samples may provide an indicator of the pathological state of the sample [65]. Benial et al. investigated the dynamic nuclear polarization properties of nitroxyl radicals used in Overhauser-enhanced MRI for simultaneous molecular imaging. [66]. The dynamic nuclear polarization (DNP) studies of redox-sensitive nitroxyl spin probes in liposomal solution reveals that the OMRI can be used to differentiate between the intra- and extra- membrane water by loading the liposome vesicles with a lipid-permeable nitroxyl spin probe [67].

Vianello et al. reported that the effects of ring structure and charge of nitroxides on the rate of decay in vivo are similar to those observed in vitro. The uncharged and negatively charged nitroxides are retained in brain, while the positively charged nitroxides are not retained in the brain, might be useful for imaging the extra cellular compartment both in NMR and ESR imaging [68]. The negatively charged spin probe, MC PROXYL is fairly lipophilic and can permeate through the BBB to brain, which can monitor the changes of the physiological redox state in the brain and the damage of the brain function caused by X ray irradiation [69]. The ESR and OMR image intensities correlated with the ESR parameters, mainly the mobility or rotational correlation time controls the enhancement and resolution of ESR/OMR images [70]. Recent studies revealed that the ESR parameters depend on physical and chemical properties of free radicals [71]. These DNP parameters depend on the ESR parameters such as line width, line shape, hyperfine coupling constant, g-factor and rotational correlation time.

The main objectives of this study are stated as follows:

- To analyze the stability of the nitroxyl radical

- To choose the suitable nitroxyl spin probe for in vivo/in vitro studies
- To optimize the liposome concentration for phantom studies
- To understand the molecular dynamics of the nitroxyl radical in high viscous medium
- To observe the DNP parameters of the nitroxyl radical in high viscous medium
- To analyze the optimal concentration of nitroxyl radical for in vivo/in vitro studies

In this work, the ESR investigations are carried out on permeable, partially permeable and impermeable nitroxyl radicals in pure water, liposomal solution and high viscous medium using multi frequency ESR spectrometers, which will be useful for optimizing the ESR/OMR imaging parameters. In addition, the DNP studies are also carried out for nitroxyl radical in high viscous medium.

Chapter I describes a brief introduction on the basic theory related with Electron spin resonance spectroscopy and dynamic nuclear polarization. The scope of the present work and literature review is also presented.

Chapter II describes the ESR and DNP measurements using ESR spectrometer and Overhauser-enhanced magnetic resonance imaging technique. The nitroxyl radicals used in this work is also reported.

Chapter III describes the electron spin resonance (ESR) spectroscopy studies on the reduction process of nitroxyl radicals were reported for 1mM concentration of ^{14}N-labeled nitroxyl radicals in 1 mM concentration of ascorbic acid as a function of time. The half life time and decay rate were estimated for 1mM concentration of ^{14}N labeled nitroxyl radicals in 1 mM

concentration of ascorbic acid. From the results, the increase in half life time and decrease in decay rate were calculated for TEMPONE compared with TEMPO and TEMPOL radicals, which indicates the higher stability of TEMPONE radical. The observed radical scavenging activity is also higher for TEMPONE radical. The ESR spectrum was also recorded for 1mM concentration of ^{14}N-labeled nitroxyl radicals in pure water and the ESR parameters, line width, hyperfine coupling constant, g-factor, signal intensity ratio and rotational correlation time were obtained. These results indicate that the TEMPONE radical has narrowest line width and fast tumbling motion compared with TEMPO and TEMPOL. Therefore, this study reveals that the TEMPONE radical can act as a good redox sensitive spin probe for molecular imaging.

Chapter IV describes the electron spin resonance (ESR) studies for 2 mM ^{14}N-labeled deuterated 3-methoxycarbonyl-2,2,5,5-tetramethyl-pyrrolidine-1-oxyl (MC-PROXYL) and 3-carboxy-2,2,5,5,-tetramethyl-pyrrolidin-1-oxyl (carboxy- PROXYL) in pure water and various concentrations of liposomal solution by using an L-band ESR spectrometer. The ESR parameters, such as the line width, hyperfine coupling constant, g-factor, rotational correlation time and partition parameter, were reported for the samples. The changes in the line width were observed for ^{14}N-labeled deuterated MC-PROXYL and carboxy-PROXYL in liposomal solution. The hyperfine coupling constant was observed for both nitroxyl spin probes. The permeable and impermeable nature of nitroxyl radicals was demonstrated using the ESR L-band spectra. The rotational correlation time increases with increasing concentration of liposome. The partition parameter for ^{14}N-labeled deuterated MC-PROXYL in liposomal solution increases with increasing concentration of liposome, which reveals that the nitroxyl spin probe permeates into lipid membrane. The lipid peaks were observed for 2 mM ^{14}N-labeled deuterated MC-PROXYL in 200, 300 and 400 mM liposomal concentration.

The lipid peaks were not observed for ^{14}N-labeled deuterated carboxy-PROXYL. These results indicate the permeable and impermeable nature of ^{14}N-labeled deuterated nitroxyl spin probe.

C**hapter V** presents the electron spin resonance (ESR) studies for 2mM ^{14}N-labeled deutrated 3-methoxycarbonyl-2,2,5,5-tetramethyl-pyrrolidine-1-oxyl (MC-PROXYL) and 3–carboxy-2,2,5,5,-tetramethyl-1-pyrrolidinyloxy (carboxy-PROXYL) in pure water and various concentrations of liposomal solutions by using 300 MHz ESR spectrometer. The ESR parameters such as the line width, hyperfine coupling constant, rotational correlation time, g-factor, partition parameter and permeability were reported for the samples. The line width broadening was observed for MC-PROXYL and carboxy-PROXYL in liposomal solution. The hyperfine coupling constant was observed for both nitroxyl spin probes. The permeable and impermeable nature of nitroxyl spin probes was demonstrated. The rotational correlation time increases with increasing concentration of liposome. The partition parameter increases with increasing concentration of liposome for MC-PROXYL, which indicates that the nitroxyl spin probes diffuse into lipid membrane. The permeability (R) value decreases with increasing concentration of liposome, which reveals that the increase of membrane permeability. The peaks correspond to lipid phase were observed for MC-PROXYL in liposomal solution, but that peak was not resolved for carboxy-PROXYL. These results confirm the permeable and the impermeable nature of nitroxyl spin probes.

C**hapter VI** presents the mobility studies on ^{14}N-labeled TEMPONE, TEMPO, carbamoyl-PROXYL, carboxy-PROXYL in high viscous liquid medium. The ESR parameters, such as line width, signal intensity ratio, g-factor, hyperfine coupling constant and correlation time were determined. The line width broadening increases two fold in high viscous samples of ^{14}N-labeled carbamoyl-PROXYL and carboxy-PROXYL, but this line

broadening is negligibly small in the high viscous sample (85% glycerol) of ^{14}N-labeled TEMPO radical. The correlation time also increases (~30 times) in the high viscous sample (85% glycerol) of ^{14}N-labeled carbamoyl-PROXYL and carboxy- PROXYL, but there is no considerable increase in the high viscous sample of ^{14}N-labeled TEMPO. TEMPONE has the narrowest line width and is also highly sensitive to viscosity. The correlation time increases (~13 times) in the high viscous sample (85% glycerol) of ^{14}N-labeled TEMPONE. Therefore, this study reveals that the ^{14}N-labeled TEMPONE radical is the most suitable spin probe for in vivo studies in high viscous biological fluids.

Chapter VII describes the dynamic nuclear polarization (DNP) studies of ^{15}N labeled carbamoyl-PROXYL in pure water and pure water/glycerol mixtures of different viscosities (1.8 cP, 7 cP and 14 cP). The dependence of DNP parameters was demonstrated over a range of agent concentration, viscosities, RF power levels and ESR irradiation time. DNP spectra were also recorded for 2 mM concentration of ^{15}N labeled cabamoyl-PROXYL in pure water and pure water/glycerol mixtures of different viscosities. The DNP factors were measured as a function of ESR irradiation time, which increases linearly upto 2 mM agent concentration in pure water and pure water/glycerol mixtures of different viscosities. The DNP factor started declining in the higher concentration region (~3 mM), which is due to the ESR line width broadening. The water proton spin-lattice relaxation time was measured at very low Zeeman field (14.529 mT). The increased DNP factor (35%) was observed for solvent 2 (η=1.8 cP) compared with solvent 1(η=1 cP). The increase in the DNP factor was brought about by the shortening of water proton spin-lattice relaxation time of solvent 2. The decreased DNP factors (30% and 53%) was observed for solvent 3 (η=7 cP)and solvent 4(η=14 cP) compared with solvent 2, which is mainly due to the low value of coupling parameter in high viscous liquid samples. The longitudinal relaxivity, leakage factor and coupling parameter were estimated. The coupling parameter values reveal that the

interactions are purely dipolar. The longitudinal relaxivity increases with the increasing viscosity of pure water/glycerol mixtures. The leakage factor showed an asymptotic increase with the increasing agent concentration. It is envisaged that the results reported here may provide guidelines for the design of new viscosity prone nitroxyl radicals, suited to the biological applications of DNP.

Chapter VIII presents the summary and conclusions of the thesis entitled “ESR studies on permeable and impermeable nitroxyl radicals used in imaging techniques”.

REFERENCES

[1] E. Zavoiskii, Journal of Physics **8**, 377 (1944)

[2] J. A. Weil, J. R. Bolton, Electron Paramagnetic Resonance-Elementary Theory and practical applications, Second Ed., (John Wiely & Sons, Hoboken, New Jersy, 2007)

[3] N. M. Atherton, Principles of Electron spin Resonance, (Ellis Horword PTR, Prentice Hall, Neywork, 1993)

[4] W. Gordy, Theory and Applications of Elecron spin Resonance, (Wiley&Sons, New York, 1980)

[5] K.M. Salikhov, Appl. Magn. Reson. **38**, 237 (2010)

[6] C. P. Poole, Electron Spin Resonance: A comprehensive Treatise on Experimental Techniques, 2 nd ed., (John Wiley&Sons, New York, 1983)

[7] D. M. Murphy, EPR (Electron Paramagnetic Resonance) Spectroscopy of Polycrystalline Oxide Systems, in Metal Oxide Catalysis (eds S. D. Jackson and J. S. J. Hargreaves), Wiley-VCH Verlag GmbH & Co. KGaA, Weinheim, Germany (2008)

[8] A. Schweiger, G. JeschkePrinciples of pulse Electron paramagnetic Resonance, (Oxford University Press, Oxford, 2001)

[9] F. Gerson, W. Huber, Electron Spin Resonance Spectroscopy of Organic Radicals, (WILEY-VCH Verlag GmbH & Co. KGaA, Weinheim, 2003)

[10] P. H. Rieger, Electron Spin Resonance Analysis and Interpretation, (The Royal Society of Chemistry, Thomas Graham House, Science Park, Milton Road, Cambridge CB4 0WF, UK, 2007)

[11] P.G. Fajer, Electron Spin Resonance Spectroscopy Labeling in Peptide and Protein Analysis, (John Wiley & Sons Ltd 2006)

[12] N. M. Atherton, Principles of Electron spin Resonance, (Ellis Horword PTR, Prentice Hall, Neywork, 1993)

[13] W. Gordy, Theory and Applications of Elecron spin Resonance, (Wiley&Sons, New York, 1980)

[14] D. M. Murphy EPR (Electron Paramagnetic resonance) Spectroscopy of polycrystalline oxide systems, Edited by S. David Jackson and Justin S. J. Hargreaves, (Wiley-VCH Verlag GmbH & Co. KGaA, Weinheim 2009)

[15] G. Jeschke, in: "Advanced ESR Methods in Polymer Research" (Ed. S. Schlick), Site-Specific Information on Macromolecular Materials by Combining CW and Pulsed ESR on Spin Probes, (Wiley, New York, 2006)

[16] P. F. Knowles, D. Marsh, Magnetic Resonance of Biomolecules: An Introduction to the Theory and Practice of NMR and ESR in Biological systems (Wiley, London 1976)

[17] R. Bartucci, D.A. Erilov, R. Guzzi, L. Sportelli, S.A. Dzuba, D. Marsh, Chem. Phys. Lipids **141**, 14 (2006)

[18] D. Marsh, Appl. Magn. Reson. **31**, 387 (2007)

[19] M. D. Lingwood, T. A. Siaw, N. Sailasutu, B. D. Ross, P. Bhattacharya, S. Han, J. Magn.Reson. **205**, 247 (2010)

[20] S. Garcia, J. H. Walton, B. Armstrong, S. Han, M. J. McCarthy, J. Magn.Reson. **203**, 138 (2010)

[21] M. D. Lingwood, A. J. Sederman, M. D. Mantle, L. F. Gladden, Songi Han, J. Magn.Reson. **216**, 94 (2012)

[22] M. Yamato, T. Shiba, T. Naganuma, K. Ichikawa, H. Utsumi, K. Yamada, Neurochem. Int. **59**, 804 (2011)

[23] O. V. Efimova, Z. Sun, S. Petryakov, E. Kesselring, G. L. Caia, D. Johnson, J. L. Zweier, V. V. Khramtsov, A. Samouilov, J. Magn. Reson. **209**, 227 (2011)

[24] G. L. Caia, O.V. Efimova, M. Velayutham, M. A. El-Mahdy, T. M. Abdelghany, E. Kesselring, S. Petryakov, Z. Sun, A. Samouilov and J. L. Zweier, J. Magn.Reson. **216**, 21 (2012)

[25] Y. Kinoshita, K. Yamada, T. Yamasaki, F. Mito, M. Yamato, N. Kosem, H. Deguchi, C. Shirahama, Y. Ito, K. Kitagawa, N. Okukado, K. Sakai and H. Utsumi, Free Radic. Biol. Med. **49**, 1703 (2010)

[26] H. G. Fujii, H. Sato-Akaba, M.C Emoto, K. Itoh, Y. Ishihara and H. Hirata, Magn. Reson. Imaging **31**, 130 (2013)

[27] O. V. Efimova, G. L. Caia, Z. Sun, S. Petryakov, E. Kesselring, A. Samouilov, J. Magn.Reson. **212**, 197 (2011)

[28] V.V. Khramtsov, G. L. Caia, K. Shet, E. Kesselring, S. Petryakov, J. L. Zweier, a. Samouilov, J. Magn.Reson. **202**, 267 (2010)

[29] M. D. Lingwood, S. Han, J. Magn.Reson. **201**, 137 (2009)

[30] L. J. Berliner, In vivo EPR (ESR) Theory and application, Biological Magnetic Resonance Vol 18, (Kluwer Academic /Plenum Publishers, New York 2003)

[31] N. Nestle, K. Shet and D. J. Lurie, Magn. Reson. Imaging **23**, 183 (2005)

[32] P.L De Sousa, R.E. De Souza, M. Engelsberg and L.A. Colnago, J. Magn. Reson.**118**, 118 (1998)

[33] D. Grucker, T. Gilberteau, B. Eclancher, J. Chambron, R. Chiarelli, A. Rassat, G. Subra and B. Gallez, J. Magn. Reson. **106**, 101 (1995)

[34] L. Mainali, M. Raguz and W. K. Subczynski, Biophys. J. **101**, 837 (2011)

[35] F. M. Megli, L. Russo and E. Conte, Biochim. Biophys. Acta. (BBA)-Bio Membranes **1788**, 371 (2009)

[36] P. Kuppusamy, M. Chzhan, K. Vij, M. Shteynbuk, D. J. Lefer, E. Giannella, L. Zweier, Proc. Natl. Acad. Sci. USA, **91**, 3388 (1994)

[37] K. Kasazaki, K. Yasukawa, H. Sano, K. Yamada, H. Utsumi, Appl. Magn. Reson. **23**, 585 (2003)

[38] F. Hyodo, R. Murugesan, K. Matsumoto, E. Hyodo, S. Subramanian, J. B. Mitchell, M. C. Krishna J. Magn. Reson. **190**, 105 (2008)

[39] S. Matsumoto, H. Utsumi, T. Aravalluvan, K.Matsumoto, A.Matsumoto, N. Devasahayam, A. L. Sowers, J. B. Mitcyhell, S. Subramanian, M. C. Krishna, J. Magn. Reson. Med. **54**, 213 (2005)

[40] D. Kruk, J. Kowalewski, D. S. Tipikin, J. H. Freed, M. Moscicki, A. Mielczarek, M.Port, J. Chem. Phys., **134,** 024508 (2011)

[41] J. Raffi, S. Gelly, L. Barral, F. Burger, P. Piccerelle, M. Prinderre, M. Boron and A. Chamayou, Spectrochim Acta, Part A: Mol Biomol Spectros. **58**, 1313 (2002)

[42] D. J. Lurie and K. Mader, Adv. Drug Deliv. Rev. **57**, 1171 (2005)

[43] K. Sakai, K. Yamada, T. Yamasaki, Y. Kinoshita, F. Mito, H. Utsumi, Tetrahedron **66**, 2311 (2010)

[44] K. Ondrias, J. Pharmaceut. Biomed. **7**, 649 (1989)

[45] M. Yamato, T. Egashira and H. Utsumi, Free Radic. Biol.Med. **35**, 1619 (2003)

[46] H. Li, Y. Deng, G.He, P. Kuppusamy, D.J. Lurie, J.L. Zweier, Magn. Reson. Med. **48**, 530 (2002)

[47] M. Yamato, T. Shiba, K. Yamada, T. watanabe, H. Utsumi, J. Cereb. Blood Flow metab. **29**, 1655 (2009)

[48] R. Franco, O.J. Schoneveld, A. Pappa and M. I. Panayiotidis, Arch Physiol Biochem. **113**, 234 (2007)

[49] R.M. Davis, J. B. Mitchell and M.C. Krishna, Anticancer agents Med. Chem. **11**, 347 (2011)

[50] R.M. Davis, A.L. Sowers, W. Degraff, M. Bernardo, A. Thetford, M.C Krishna and J.B Mitchell, Free Radic. Biol. Med. **51**, 780 (2011)

[51] K. Anzai, K. Saito, K. Takeshita, S. Takahashi, H. Miyazaki, H. Shoji, M. Lee, T. Masumizu, T. Ozawa, Mag. Reson. Imaging, **21**, 765 (2003)

[52] W. Froncisz, J.S. Hyde, J. Magn. Reson. **47**, 515 (1982)

[53] S. J. Lukiewicz, S. G. Lukiewicz, Magn. Reson. Med. **1**, 297 (1984)

[54] L. J. Berliner, H. Fujii, Science **227**, 517 (1985)

[55] L. J. Berliner, H. Fujii, X. Wan, S. J. Lukiewicz, Magn. Reson. Med. **4**, 380 (1987)

[56] L. J. Berliner, H. Fujii, Biol. Magn. Reson. **11**, 307 (1992)

[57] M. Ono, T. Ogata, K. C. Hsieh, M. Suzuki, E. Yoshida, H. Kamada, Chem. Lett. **15**, 491 (1986)

[58] A. Stogiu, J. Magn. Reson. **65**, 206 (1985)

[59] M. J. Nilges, T. Walczak, Swartz. HM, Phys. Med. **2**, 195 (1989)

[60] H. Hirata, H. Iwai, M. Ono, Rev. Sci. Instrum. **66**, 4529 (1995)

[61] N. Kosem, T. Naganuma, K. Ichikawa, N. P. Morales, K. Yasukawa, F. Hyodo, K. Yamada, H. Utsumi, Free Radical Bio. Med. **53**, 328 (2012)

[62] A. Tomizawa, I. Ishii, Z. Zhelev, I. Aoki, S. Shibata, M. Kitada, R. Bakalova, Biochimica et Biophysics Acta, **1810**, 1309 (2011)

[63] J. Han, K. Takeshita, H. Utsumi, Free Radical Bio. Med. **30**, 516 (2001)

[64] H. Utsumi, K. Yasukawa, T. Soeda, K. Yamada, R. Shigemi, T. Yao, M. Tsuneyoshi, J. Pharmacol. Exp. Ther. **317**, 228 (2006)

[65] I. Nicholson, D.J. Lurie, F.J.L. Robb, J. Magn. Reson. Ser. B **104**, 250 (1994)

[66] A. Milton Franklin Benial, K. Ichikawa, R. Murugesan, K. Yamada and H. Utsumi, J. Magn. Reson. **182**, 273 (2006)

[67] A. Milton Franklin Benial, H. Utsumi, K. Ichikawa, R. Murugesan, K. Yamada, Y. Kinoshita, T. Naganuma, M. Kato, J. Magn. Reson. **204**, 131 (2010)

[68] F. Vianello, F. Momo, M. Scarpa, A. Rigo, Mag. Reson. Imaging **13**, 219 (1995)

[69] Y. Miura, K. Anzai, S. Takahashi, T. Ozawa, FEBS Letters **419**, 99 (1997)

[70] H. Utsumi, K. Yamada, K. Ichikawa, K. Sakai, Y. Kinoshita, S. Matsumoto, M. Nagai, Proc. Natl. Acad. Sci. USA **103**, 1463 (2006)

[71] M.C. Krishna, S. English, K. Yamada, J. Yoo, R. Murugesan, N. Devasahayam J.A. Cook, K. Golaman, J.H. Ardenkjaer-Larsen, S. Subramanian, J.B. Mitchell, Proc. Natl. Acad. Sci. USA **99**, 2216 (2002)